Novel Tin(IV) Complexes with the Hybrid Guanidine Ligand DMEGqu

Anton Jesser[a], Ines dos Santos Vieira[b] and Sonja Herres-Pawlis[a]

[a] Department Chemie, Ludwig-Maximilians-Universität München, Butenandtstraße 5 – 13, 81377 München, Germany

[b] Anorganische Chemie II, Technische Universität Dortmund, Otto-Hahn-Straße 6, 44227 Dortmund, Germany

Reprint requests to Sonja Herres-Pawlis. Fax: (+49)089-218077904.
E-mail: Sonja.Herres-Pawlis@cup.uni-muenchen.de

Z. Naturforsch. **2013**, *68b*, 653 – 665 / DOI: 10.5560/ZNB.2013-3080
Received March 5, 2013

Dedicated to Professor Heinrich Nöth on the occasion of his 85th birthday

Novel Sn(IV) complexes with the guanidine-quinoline hybrid ligand DMEGqu are reported. With $SnCl_4$, $SnBr_4$, Me_2SnCl_2, Me_2SnBr_2, and the 3,5-di-*tert*-butyl-catecholate coligand complexes with different donor sets were synthesized. Four of these tin compounds have been modelled by density functional theory. Additionally, a tetranuclear Sn(IV) oxocluster with a novel structure motif, a distorted hetero-adamantane with bridging oxido and hydroxido ligands, is presented.

Key words: Guanidine Ligands, Tin Complexes, X-Ray Diffraction, Density Functional Theory

Introduction

Since 1969 adducts of tin(IV) with pyridine are known [1], and hitherto coordination compounds with numerous *N*-donor ligands have been characterized [2 – 7]. In addition to the *N*-donor function, mixed complexes with other donors like oxygen, sulfur or with organotin precursors are commonly found [2 – 7]. Among the *N*-donor ligands, C=N double bonds prevail with the scope spanning simple imines, Schiff bases and amidinates, as well as heterocyclic nitrogen ligands containing pyrazoles, imidazoles, pyridine and related compounds. Besides kind and strength of donor, also the denticity of the ligand is variable, commonly ranging from mono- to tridentate. With a tetradentate ligand, Fukuzumi and Kojima recently reported on an octahedral Sn(IV) dodecaphenylporphyrin complex being only one in a large series of complexes with porphyrin derivates [8]. Octahedrally coordinated Sn(IV) complexes with Schiff base ligands and an additional quinoline donor function were reported by Shibahara *et al.* [9]. Di- and triorganotin(IV) complexes with Schiff bases, bipyridine and phenanthrolines have been studied on behalf of their biological relevance, such as nematicidal, insecticidal and antifertility activities [10]. Complexes with ligands combining different donor types lead to a great variety of donor sets and coordination geometry. Besides the six-coordinate octahedral geometry, trigonal-bipyramidal (five-coordinate) and pentagonal-bipyramidal (seven-coordinate) geometries have been reported [11, 12].

In spite of the large number of known Sn(IV) complexes with *N*-donor ligands, a search of the Cambridge Structural Database yielded no results of Sn(IV) complexes with neutral guanidine ligands. Several complexes with anionic guanidinate ligands were found [13, 14], but the Sn(IV) coordination chemistry with neutral guanidines seems to be completely unexplored.

Guanidines have proven to be a versatile ligand class suitable for stabilization of various transition metals in both high and low oxidation states [15 – 19]. The combination of the guanidine moiety with further aliphatic or aromatic *N*-donor functions leads to the hybrid guanidine ligand class, which allows adjusting the donor moieties to the electronic situation of a central metal atom. Thus, it is possible to distribute a high formal charge of a central metal atom within the guanidine moiety by delocalization of the C=N double bond, or to stabilize an electron-rich central metal atom by allocating electron density to the electron-deficient aromatic *N*-donor function of the

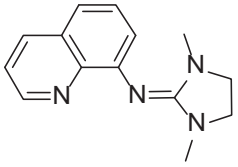

Fig. 1. Hybrid guanidine ligand DMEGqu.

quinoline [15 – 19]. The nature of the central atom influences on the nitrogen-metal bond lengths. For Sn(IV) with its high formal charge, the involvement of the guanidine in the binding situation should be greater than for a low-valent transition metal.

Here we present complexes of the guanidine-quinoline hybrid ligand *N*-(1,3-dimethylimidazolidin-2-ylidene)quinoline-8-amine (DMEGqu) [20, 21] (Fig. 1) with tin in its oxidation state +4 which represent the first tin guanidine compounds reported so far. As starting compounds $SnCl_4$, $SnBr_4$, Me_2SnCl_2, and Me_2SnBr_2 were used.

Furthermore, the molecular structure of a novel tetranuclear Sn(IV) oxocluster is presented. The four chemically equivalent Sn atoms are coordinated by four bridging oxido and two additional hydroxido ligands, thus forming a distorted hetero-adamantane cage. Additionally, the Sn atoms are coordinated by the bidentate *N*-donor ligand DMEGqu, rendering this cluster the first reported adamantane-like structure in tin coordination chemistry.

Results and Discussion

Synthesis and molecular structures of hybrid guanidine tin complexes

Via reaction of $SnCl_4$, Me_2SnCl_2 and Me_2SnBr_2 with the ligand DMEGqu three neutral monochelate complexes [Sn(DMEGqu)Cl_4] (**C1**), [Me_2Sn(DMEGqu)Cl_2] (**C2**) and [Me_2Sn(DMEGqu)Br_2] (**C3**) were obtained (Scheme 1). Additionally, the neutral complex [Sn(DMEGqu)(3,5-DBCat)Cl_2] · 1.5THF (**C4**) with 3,5-di-*tert*-butyl-catecholate (3,5-DBCat) as co-ligand was synthesized by reaction of $SnCl_2$ with 3,5-di-*tert*-butyl-*o*-benzoquinone (3,5-DBQ) leading to *in situ* generation of the [Sn(thf)$_2$(3,5-DBCat)Cl_2] complex, and the following reaction with DMEGqu (Scheme 2) [22]. The molecular structures of these complexes were determined *via* single-crystal X-ray structure analysis. Additional characterization was accomplished with IR spectroscopy, mass spectrometry and elemental analysis.

Furthermore, we present the structure of the tetranuclear dicationic tin oxocluster [(Sn(DMEGqu)Br)$_4$(μ_2-O)$_4$(μ_2-OH)$_2$]Br_2 · 2MeCN (**C5**), obtained *via* hydrolysis (Scheme 3) of an intermediate DMEGqu complex with $SnBr_4$ which could not be structurally characterized. Further characterization of the oxocluster could not be accomplished due to a very small yield. Consecutive attempts at resynthesis were not successful.

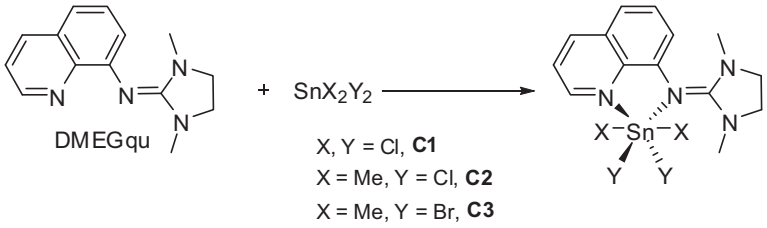

Scheme 1. General synthesis of hybrid guanidine tin complexes **C1**–**C3**.

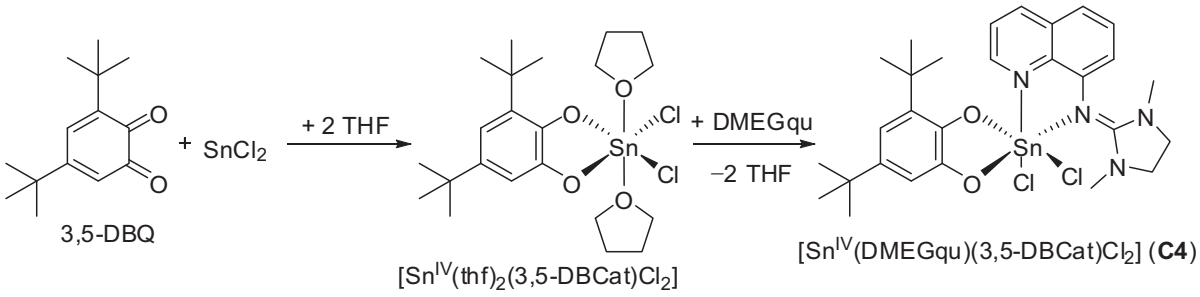

Scheme 2. Synthesis of the Sn(IV) catecholate complex [Sn(DMEGqu)(3,5-DBCat)Cl_2] · 1.5THF (**C4**).

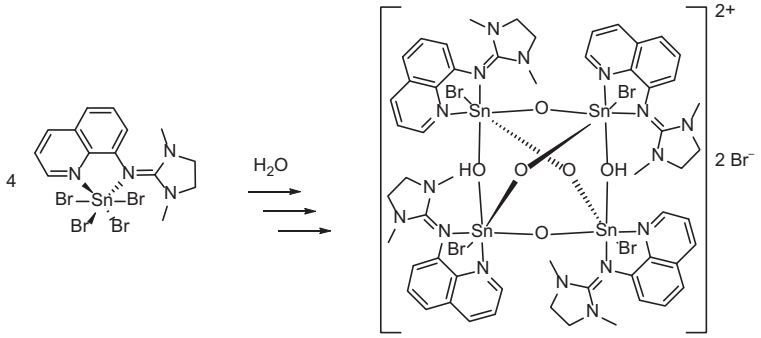

Scheme 3. Synthesis of the tin oxocluster $[(Sn(DMEGqu)Br)_4(\mu_2\text{-}O)_4(\mu_2\text{-}OH)_2]Br_2 \cdot 2MeCN$ (**C5**).

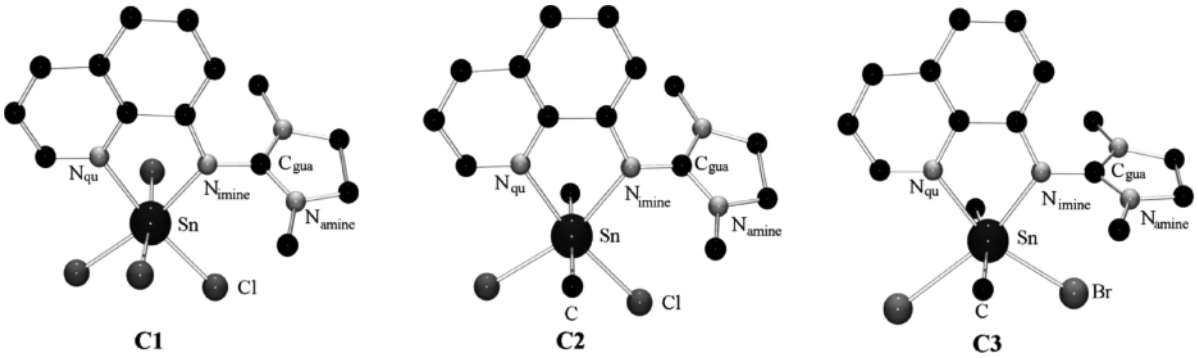

Fig. 2. Molecular structures of $[Sn(DMEGqu)Cl_4]$ (**C1**), $[Me_2Sn(DMEGqu)Cl_2]$ (**C2**) and $[Me_2Sn(DMEGqu)Br_2]$ (**C3**) in the solid state (hydrogen atoms are omitted for clarity).

Table 1. Selected bond lengths (Å) and angles (deg) of the complexes **C1**, **C2** and **C3**.

	$[Sn(DMEGqu)Cl_4]$ (**C1**)	$[Me_2Sn(DMEGqu)Cl_2]$ (**C2**)	$[Me_2Sn(DMEGqu)Br_2]$ (**C3**)
Bond lengths			
$Sn–N_{imine}$	2.150(2)	2.319(3)	2.239(3)
$Sn–N_{qu}$	2.209(2)	2.322(3)	2.333(3)
Sn–X	2.401(1), 2.377(1) 2.405(1), 2.414(1)	2.553(1), 2.568(1)	2.934(1), 2.697(1)
Sn–C	–	2.130(3), 2.138(3)	2.115(3), 2.116(4)
$C_{gua}–N_{imine}$	1.367(3)	1.354(5)	1.353(5)
$C_{gua}–N_{amine}$	1.317(3), 1.323(3)	1.335(6), 1.336(5)	1.329(4), 1.317(5)
Bond angles			
N–Sn–N	76.0(1)	71.6(1)	72.3(1)
X–Sn–X	96.9(1)	100.3(1)	107.9(2)
Guanidine key parameters			
$\angle$ ($N_{amine}C_3$, $C_{gua}N_3$)	2.7 (av)	6.8 (av)	4.4 (av)
ρ[a]	1.04	1.01	1.02

[a] $\rho = 2a/(b+c)$ with $a = d(C_{gua}{=}N_{imine})$, b and $c = d(C_{gua}{-}N_{amine})$ [23].

The molecular structures of the complexes are shown in Figs. 2 – 4. Selected bond lengths and angles are given in Tables 1 and 2.

The monochelate complex $[Sn(DMEGqu)Cl_4]$ (**C1**) and the catecholate complex $[Sn(DMEGqu)(3,5\text{-}DBCat)Cl_2] \cdot 1.5THF$ (**C4**) crystallize in the monoclinic space group $P2_1/c$, the monochelate complexes $[Me_2Sn(DMEGqu)Cl_2]$ (**C2**) and $[Me_2Sn(DMEGqu)Br_2]$ (**C3**) crystallize in the orthorhombic space group $P2_12_12_1$, with four

molecules in the unit cell. The tin oxocluster $[(Sn(DMEGqu)Br)_4(\mu_2\text{-}O)_4(\mu_2\text{-}OH)_2]Br_2 \cdot 2MeCN$ (**C5**) crystallizes in the monoclinic space group *C*2/*c* with four molecules in the unit cell, whereby the complex itself exhibits crystallographic C_2 symmetry.

The coordination geometry in all complexes is best described as distorted octahedral. The Sn atom is coordinated by the imine and the quinoline *N*-donor function of the hybrid guanidine ligand DMEGqu, the other coordination sites are occupied by four chlorido (**C1**), two methyl and two chlorido (**C2**) or two methyl and two bromido ligands (**C3**) (Fig. 2).

The Sn–N bond lengths in **C1** are considerably shorter than in the complexes with methyl-substituted Sn centers. This is explained by the smaller electronegativity of the methyl groups compared to the halido ligands, leading to a higher positive charge of the Sn atom in **C1** and thus to a stronger coordination of the DMEGqu ligand. In the crystal structures of the complexes **C1** and **C3** there is a significant difference between the Sn–N_{imine} bond lengths (2.150(2) Å, **C1**; 2.239(3) Å, **C3**) and the Sn–N_{qu} bond lengths (2.209(2) Å, **C1**; 2.333(3) Å, **C3**) with the Sn–N_{imine} bonds being shorter. In **C2** the Sn–N bonds are equally long (2.319(3), 2.322(3) Å). In **C1** and **C3**, we observe with different Sn–N bond lengths also different Sn–X bond lengths. The coordinating N atoms of the DMEGqu ligand show a structural *trans* influence on the coplanar halido ligands. The Sn–Cl bond lengths in **C1** amount to 2.377(1) – 2.414(1) Å. The chlorido ligand with the shortest Sn–Cl distance is in *trans* position to the longer Sn–N_{qu} bond. In **C3** a *trans*-positioned Sn–Br bond is stretched significantly due to the *trans* influence of the N_{imine} atom (2.934(1), 2.697(1) Å). In **C2** no such influence is observed. The Sn–Cl bonds are longer than in **C2** (2.553(1), 2.568(1) Å), which is ex-

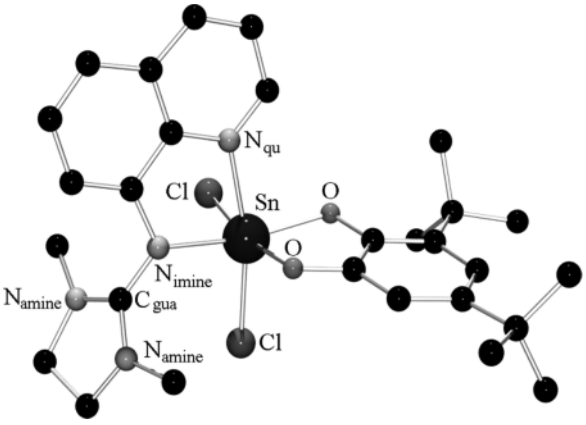

Fig. 3. Molecular structure of [Sn(DMEGqu)(3,5-DBCat)Cl_2] · 1.5THF (**C4**) in the solid state (hydrogen atoms and interstitial THF molecules are omitted for clarity).

Table 2. Selected bond lengths (Å) and angles (deg) of the complexes **C4** and **C5**.

	[Sn(DMEGqu)(DBCat)Cl_2] · 1.5THF (**C4**)	$[(Sn(DMEGqu)Br)_4(\mu_2\text{-}O)_4(\mu_2\text{-}OH)_2]Br_2 \cdot 2MeCN$ (**C5**)
Bond lengths		
Sn–N_{imine}	2.142(3)	2.184(4), 2.191(4)
Sn–N_{qu}	2.223(3)	2.234(4), 2.214(4)
Sn–X	2.388(1), 2.396(1)	2.640(1), 2.636(1)
Sn–OH	–	2.129(2), 2.170(2)
Sn–O	2.036(2), 2.061(3)	1.949(3), 1.968(3)
		1.945(2), 1.954(2)
C_{gua}–N_{imine}	1.363(5)	1.372(6), 1.356(6)
C_{gua}–N_{amine}	1.322(5), 1.332(5)	1.322(6), 1.330(6)
		1.311(6), 1.326(6)
Bond angles		
N–Sn–N	75.3(1)	73.8(2), 74.2(2)
O–Sn–O	82.1(1)	107.5(1), 106.1(1)
O–Sn–OH		89.7(1), 93.1(1)
		86.7(1), 96.7(1)
Guanidine key parameters		
$\angle$ ($N_{amine}C_3$, $C_{gua}N_3$)	4.0 (av)	3.7 (av), 3.7 (av)
ρ[a]	1.03	1.03, 1.03

[a] $\rho = 2a/(b+c)$ with $a = d(C_{gua}{=}N_{imine})$, b and $c = d(C_{gua}{-}N_{amine})$ [23].

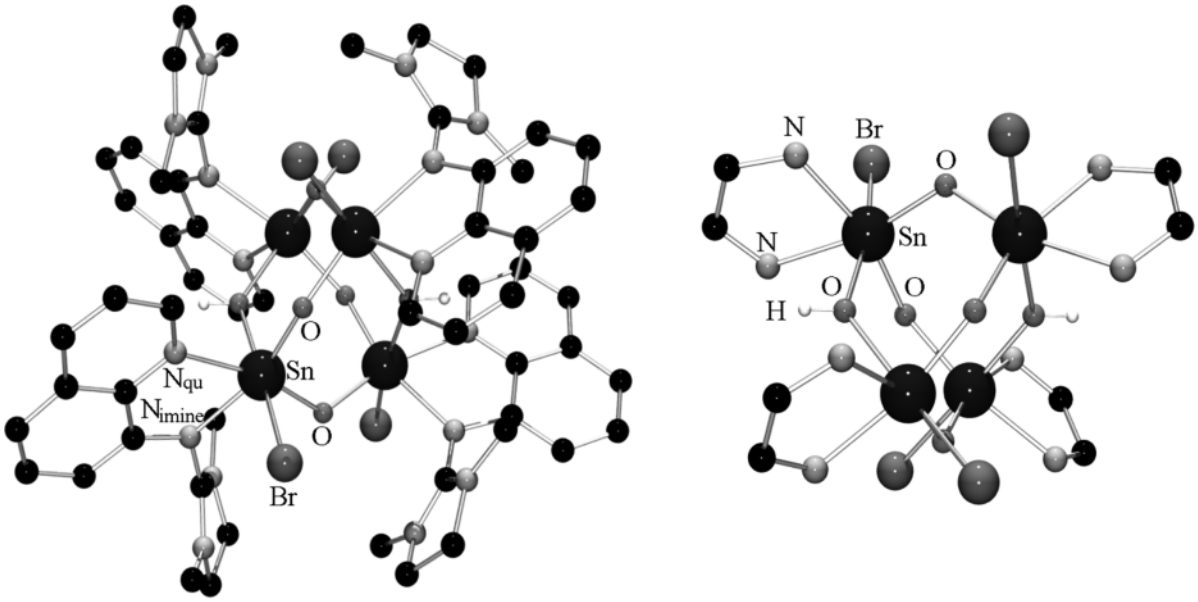

Fig. 4. left: Molecular structure of $[(Sn(DMEGqu)Br)_4(\mu_2\text{-}O)_4(\mu_2\text{-}OH)_2]Br_2 \cdot 2MeCN$ (**C5**) in the solid state (hydrogen atoms and interstitial acetonitrile molecules are omitted for clarity); right: View of the distorted adamantane-like structural motif of **C5**.

plained by the smaller positive charge on the Sn atom in **C2**. The methyl substituents are in a *trans* position to each other.

In the catecholate complex (**C4**) two coordination sites are occupied by the donor functions of the dianionic 3,5-di-*tert*-butylcatecholate ligand (3,5-DBCat) and further two by chlorido ligands (Fig. 3). The complex crystallizes with 1.5 tetrahydrofuran molecules in the asymmetric unit. In **C4** with a $SnN_2O_2Cl_2$ donor set, equal ligands are *cis*-positioned. Likewise to **C1** and **C3**, the Sn–N_{imine} bond is shorter than the Sn–N_{qu} bond (2.142(3) *vs*. 2.223(3) Å). The C_{cat}–O bond lengths (1.331(4) – 1.370(5) Å) are in good agreement with C–O single bond lengths in other catecholate complexes [24].

The tetranuclear tin oxocluster (**C5**) exhibits a distorted hetero-adamantane cage, with the Sn atoms connected *via* two μ-oxido bridges and one μ-hydroxido group each (Fig. 4). This structural motif is not yet known in the literature: Related motifs are found for Sn_4S_6 adamantanes [25, 26], and there is one example for a Sn_4O_6 adamantane published by Roesky *et al*. [27]. The structure presented herein differs in two ways: first, two bridging hydroxido ligands lead to a loss of symmetry, and thus to a considerable distortion of the adamantane skeleton. Secondly, the Sn atoms in reported examples possess organic substituents and are four-coordinate, whereas in the presented oxocluster the Sn atoms are six-coordinate by the bidentate *N*-donor ligand DMEGqu and an additional bromido ligand. The adamantane core of the compounds of Roesky *et al.* is regular and highly symmetric and possesses the point group T. The asymmetric unit contains only $1/12$ of the whole molecule. The Sn atoms are four-coordinate, with three equivalent bridging oxygen atoms and a terminal tris(trimethylsilyl)methyl group showing distorted tetrahedral geometry. The Sn–O bond lengths are all equal and amount to 1.968 Å [27]. The oxocluster **C5** is far less symmetric. There is a C_2 axis which is coaxial with the O–H bonds of the hydroxido ligands, so that two of the four Sn atoms and their coordination spheres are symmetrically equivalent. Each Sn atom is six-coordinated. The coordination sites which are not part of the adamantane cage are occupied by the DMEGqu and a bromido ligand.

With respect to the coordinative situation of the DMEGqu ligand, the oxocluster **C5** shows similarities to the other complexes presented here. The Sn–N_{imine} bonds (2.184(4), 2.191(4) Å) are shorter than the Sn–N_{qu} bonds (2.234(4), 2.214(4) Å), and both are longer than the corresponding bonds in **C1** and **C4**,

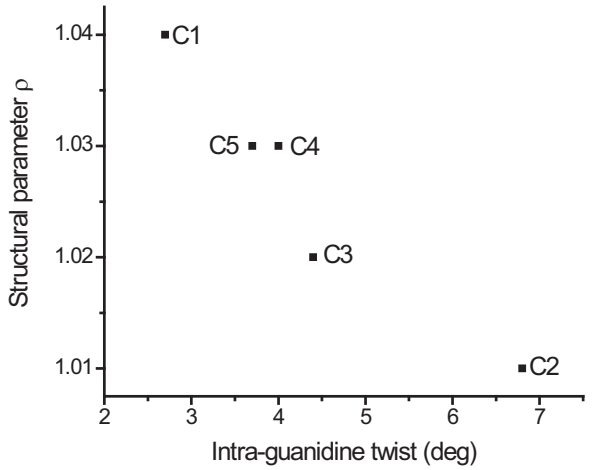

Fig. 5. Correlation of the structural parameter ρ with the *intra*-guanidine twist in complexes **C1**–**C5**.

and shorter than those in **C2** and **C3**. A reason might be the higher positive charge on the Sn atoms compared to the methyl-substituted complexes. This is as well observed in the shorter Sn–Br bonds (2.640(1), 2.636(1) Å) as compared to **C3**. The Sn–O bonds in **C5** (1.945(2) – 1.968(3) Å) are shorter than the Sn–O bonds in **C4** (2.036(2) – 2.061(3) Å) and also significantly shorter than the Sn–OH bonds (2.129(2), 2.170(2) Å). It is worth noting that the Sn–O bonds in **C5** are in good agreement with those in the regular adamantane core reported by Roesky *et al.* [27], even though there is a difference in the coordination geometry of the Sn atoms.

In known complexes with the DMEG guanidine moiety, the torsion of the $N_{amine}C_3$ planes *versus* the $C_{gua}N_3$ plane, also known as the *intra*-guanidine twist, is less pronounced than in similar complexes with other guanidines due to the bridging ethylene group of DMEG. In the literature, for transition metal complexes torsion values of about 12° are found [16, 20]. However, in the presented structures a more pronounced planarity of the DMEG moiety is observed (2.7 (av)°, **C1**; 6.8 (av)°, **C2**; 4.4 (av)°, **C3**; 4.0 (av)°, **C4**; 3.7 (av)°, **C5**). The formal $C_{gua}{=}N_{imine}$ double bonds (1.353(5) – 1.372(6) Å) are considerably longer than the C_{gua}–N_{amine} bonds (1.311(6) – 1.336(5) Å) which leads to structure parameter values of ρ greater 1.0 (1.01 – 1.04) [23]. For calculation of ρ, the formula $\rho = 2a/(b+c)$ applies, where a is the C=N bond length and b and c are the C–NR_2 bond lengths. In case of a total delocalization of the double bond within the guanidine moiety, ρ is equal one. The ρ value of the presented complexes is extremely high and correlates well with the high formal charge on the central Sn(IV) atoms. The structure parameter values of ρ correlate with the torsion values of the *intra*-guanidine twist, as shown in Fig. 5. With increasing planarity of the guanidine moiety the delocalization of the double bond within the C_{gua}–N_{amine} bonds also increases, and the double bond character of the C_{gua}–N_{imine} bond decreases.

Theoretical description of the geometries of Sn(IV) hybrid guanidine complexes

To obtain an adequate theoretical description of the synthesized Sn(IV) guanidine complexes a structural benchmarking was accomplished. Therefore the structures of the complexes [Sn(DMEGqu)Cl_4] (**C1**) and [Me_2Sn(DMEGqu)Cl_2] (**C2**) were optimized with various density functionals, and the results were compared with experimental data from X-ray analyses. The pure GGA (general gradient approximation) functionals BLYP and BP86 as well as the hybrid GGA B3LYP [22 – 31] were chosen for comparison. The Sn atoms were described with the electronic core potentials (ECPs) and basis sets from the Ahlrichs (def2-SVP, def2-TZVP) [32, 33], Hay and Wadt (LANL2DZ) [34] and the Stuttgart (ECP46MWB_VTZ) [35] groups. The description of the first and second row atoms was performed with Pople basis sets (6-31G(d), 6-311G(d) [36]. Selected bond lengths and angles of the calculated structures are summarized in Tables 3 and 4. For reasons of comparison the relative deviation from experimental values is given.

The DFT results show that the theoretical description of the complexes **C1** and **C2** *via* use of double-ζ und triple-ζ basis sets developed by Pople and Ahlrichs exhibits considerable deviation from the experimental values. The Sn–N bond lengths are altogether overestimated and the Sn–N_{imine} bond lengths are predicted with higher values than the Sn–N_{qu} bond lengths, whereas for **C1** the inverse case is observed and for **C2** no relevant difference in Sn–N bond lengths is found. The deviations in Sn–N_{imine} bond lengths amount to 7.4 – 12.0 % for **C1** (13.5 – 25.4 %, **C2**), while for Sn–N_{qu} bonds deviations of 3.7 – 6.4 % for **C1** (8.0 – 13.9 % for **C2**) have been found. Overall, cal-

Table 3. Selected bond lengths (Å) and deviations (%) of optimized structures of [Sn(DMEGqu)Cl_4] (**C1**).

		$Sn–N_{imine}$ (Å)	Dev. (%)	$Sn–N_{qu}$ (Å)	Dev. (%)	$C_{gua}–N_{imine}$ (Å)	Dev. (%)	$C_{gua}–N_{amine}$ (av) (Å)	Dev. (%)
Crystal structure		2.150		2.209		1.367		1.321	
Def2-SVP	B3LYP	2.346	9.1	2.314	4.8	1.345	−1.6	1.351	2.3
	BLYP	2.408	12.0	2.351	6.4	1.352	−1.1	1.366	3.4
	BP86	2.357	9.6	2.316	4.8	1.350	−1.2	1.361	3.0
Def2-SVP/	B3LYP	2.333	8.5	2.308	4.5	1.350	−1.2	1.350	2.2
6-31G(d)	BLYP	2.390	11.2	2.342	6.0	1.358	−0.7	1.365	3.4
	BP86	2.348	9.2	2.313	4.7	1.355	−0.9	1.361	3.0
Def2-TZVP	B3LYP	2.319	7.9	2.290	3.7	1.345	−1.6	1.343	1.7
	BLYP	2.381	10.7	2.327	5.3	1.353	−1.0	1.359	2.9
	BP86	2.335	8.6	2.294	3.8	1.350	−1.2	1.354	2.5
Def2-TZVP/	B3LYP	2.310	7.4	2.292	3.8	1.350	−1.2	1.346	1.9
6-311G(d)	BLYP	2.368	10.1	2.327	5.3	1.358	−0.7	1.362	3.1
	BP86	2.326	8.2	2.296	3.9	1.354	−1.0	1.357	2.8
LANL2DZ	B3LYP	2.198	2.2	2.212	0.1	1.374	0.5	1.358	2.8
	BLYP	2.239	4.1	2.235	1.2	1.383	1.2	1.374	4.0
	BP86	2.225	3.5	2.224	0.7	1.377	0.7	1.369	3.7
LANL2DZ/	B3LYP	2.261	5.2	2.256	2.1	1.356	−0.8	1.348	2.0
6-31G(d)	BP86	2.287	6.4	2.268	2.7	1.360	−0.5	1.359	2.9
ECP46MWB_VTZ/	B3LYP	2.312	7.5	2.295	3.9	1.350	−1.2	1.346	1.9
6-311G(d)									

Table 4. Selected bond lengths (Å) and deviations (%) of optimized structures of [Me_2Sn(DMEGqu)Cl_2] (**C2**).

		$Sn–N_{imine}$ (Å)	Dev. (%)	$Sn–N_{qu}$ (Å)	Dev. (%)	$C_{gua}–N_{imine}$ (Å)	Dev. (%)	$C_{gua}–N_{amine}$ (av) (Å)	Dev. (%)
Crystal structure		2.319		2.322		1.354		1.336	
Def2-SVP	B3LYP	2.698	16.3	2.543	9.5	1.321	−2.4	1.364	2.1
	BLYP	2.774	19.6	2.585	11.3	1.331	−1.7	1.379	3.2
	BP86	2.647	14.1	2.510	8.1	1.332	−1.6	1.372	2.7
Def2-SVP/	B3LYP	2.709	16.8	2.547	9.7	1.324	−2.2	1.365	2.2
6-31G(d)	BLYP	2.795	20.5	2.592	11.6	1.334	−1.5	1.381	3.4
	BP86	2.653	14.4	2.519	8.5	1.336	−1.3	1.373	2.7
Def2-TZVP	B3LYP	2.802	20.8	2.580	11.1	1.314	−3.0	1.361	1.9
	BLYP	2.908	25.4	2.644	13.9	1.324	−2.2	1.376	3.0
	BP86	2.677	15.4	2.517	8.4	1.329	−1.8	1.366	2.2
Def2-TZVP/	B3LYP	2.681	15.6	2.538	9.3	1.324	−2.2	1.361	1.8
6-311G(d)	BLYP	2.770	19.4	2.587	11.4	1.333	−1.6	1.377	3.0
	BP86	2.632	13.5	2.507	8.0	1.334	−1.5	1.369	2.4
LANL2DZ	B3LYP	2.400	3.5	2.350	1.2	1.360	0.4	1.365	2.2
	BLYP	2.477	6.8	2.383	2.6	1.368	1.0	1.383	3.5
LANL2DZ/	B3LYP	2.552	10.0	2.442	5.2	1.333	−1.6	1.359	1.7
6-31G(d)	BP86	2.548	9.9	2.438	5.0	1.341	−1.0	1.369	2.5
ECP46MWB_VTZ/	B3LYP	2.660	14.7	2.529	8.9	1.326	−2.1	1.359	1.7
6-311G(d)									

culations with the hybrid GGA B3LYP provide the best results.

The description of the C–N bonds of the guanidine moiety is more accurate, with deviations of −1.6 to 3.4 % (**C1**) and −3.0 to 3.4 % (**C2**). However, the much longer $C_{gua}–N_{imine}$ as compared to the $C_{gua}–N_{amine}$ bond lengths are not predicted correctly with Pople and Ahlrichs basis sets but only at the relatively simple level of theory B3LYP/LANL2DZ. The best description of the Sn–N bond lengths is also achieved with LANL2DZ. A combination of LANL2DZ with a Pople basis (6-31G(d)) for the lighter atoms did not provide better results, as well as the use of the Stuttgart pseudopotential ECP46MWB_VTZ. Hence, the coordination situation of tin guanidine complexes seems to be a theoretical challenge: Only the sim-

Table 5. Selected bond lengths (Å) of optimized structures of **C1**–**C4** at the B3LYP/LANL2DZ level of theory.

	[Sn(DMEGqu)Cl_4] (**C1**)	[Me_2Sn(DMEGqu)Cl_2] (**C2**)	[Me_2Sn(DMEGqu)Br_2] (**C3**)	[Sn(DMEGqu)(DBCat)Cl_2] (**C4**)
Sn–N_{imine}	2.198	2.400	2.381	2.177
Sn–N_{qu}	2.212	2.350	2.341	2.215
Sn–Cl	2.457−2.508	2.593, 2.624	2.487, 2.492	–
Sn–Br	–	–	2.806, 2.837	–
Sn–Me	–	2.131, 2.135	2.138, 2.140	–
Sn–O	–	–	–	2.007, 2.019
C_{gua}–N_{imine}	1.374	1.360	1.364	1.372
C_{gua}–N_{amine}	1.352	1.357	1.356	1.350
Sn–O	1.363	1.373	1.370	1.360

ple LANL2DZ basis describes it reasonably well – by chance.

The structures of the complexes **C1**–**C4** were optimized at the B3LYP/LANL2DZ level of theory. Harmonic frequencies of the optimized structures were calculated in order to confirm the nature of the stationary points. For **C3** and **C4** as well, good accordance to crystal structure data was found. Selected bond lengths are summarized in Table 5.

IR spectroscopy and vibrational analysis

For the complexes **C1**–**C4** vibrational analyses were performed with B3LYP/LANL2DZ. The results were compared to experimental infrared spectra. In Table 6, characteristic frequencies are listed with their theoretical assignment to specific vibrational modes. For reason of clarity, we have focused on the most intense bands. Especially, the guanidine-derived bands have been thoroughly analyzed: They can be dissected into the stretching and deformation modes of the C–N bonds and in-plane combinations thereof (Scheme 4). Thus, for **C1** the IR band at 1599 cm^{-1} has been assigned to the stretching (ν) mode of the C–N bond, while the band at 1468 cm^{-1} stems from the stretching (ν) mode of the C=N double bond. The band at 1238 cm^{-1} has been assigned to a deformation (δ) mode of the CN_3 moiety of the guanidine, and two further bands at 1408 and 1026 cm^{-1} have been assigned to combinations of stretching and deformation of the CN_3 moiety and the ethylene spacer of the DMEG group (guanidine ip A, B). All of these modes lie in the approximated plane through the DMEG, and are marked as in-plane (ip). In-plane stretching modes of the quinoline ring system are predicted in a relatively wide range (approx. 1550 – 1300 cm^{-1}) and can be assigned to several prominent IR bands of **C1** (1554, 1506, 1381 and 1302 cm^{-1}). Several C–H stretching modes are predicted for wavenumbers > 3000 cm^{-1}, and C–H deformation modes can be assigned to the bands at 1331 (guanidine) and 858 cm^{-1} (quinoline). For **C2** and **C3**, additional C–H deformation modes of the methyl substituents of the Sn atom are found at about 1270 cm^{-1}. For **C4**, the 3,5-di-*tert*-butylcatecholate ligand (DBCat) gives rise to additional C–C stretching and deformation modes around 1200 – 1300 cm^{-1}, as well as a C–O stretching mode, which can be assigned to the IR band at 980 cm^{-1}. Overall, qualitatively good accordance of the theoretical results with the experimental data has been achieved. The quantitative accordance is limited due to the small basis set yielding slightly too large wavenumbers. Frequency scaling with the typical scaling factor for B3LYP/LANL2DZ of 0.9978 [37] does not lead to

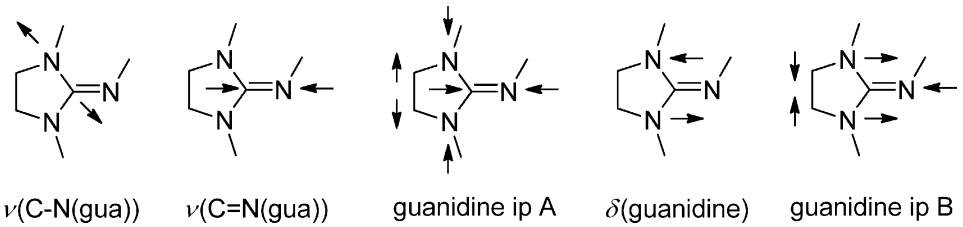

Scheme 4. Vibrational modes of the guanidine moiety.

Table 6. Experimental and calculated (B3LYP/LANL2DZ, reported unscaled) frequencies (cm^{-1}) for **C1**–**C4**[a].

[Sn(DMEGqu)Cl_4] (**C1**)			[Me_2Sn(DMEGqu)Cl_2] (**C2**)			[Me_2Sn(DMEGqu)Br_2] (**C3**)			[Sn(DMEGqu)(DBCat)Cl_2] (**C4**)		
experimental	calcd.	assignment	experimental	calcd.	assignment	experimental	calcd.	assignment	experimental	calcd.	assignment
3097	3201 – 3256	ν(C–H(qu))	3062	3194 – 3245	ν(C–H(qu))	3055	3195 – 3246	ν(C–H(qu)	2951	3198 – 3260	ν(C–H(arom))
3072	3042 – 3194	ν(C–H(gua))	3045	3039 – 3190	ν(C–H(gua))	3033	3041 – 3195	ν(C–H(gua))	2900	3024 – 3172	ν(C–H(aliph))
1599	1610	ν(C–N(gua))	1595	1599	ν(C–N(gua))	1595	1601	ν(C–N(gua))	1597	1616	ν(C–N(gua))
1554	1552	quinoline ip	1574	1572	ν(C–N(gua))	1552	1550	quinoline ip	1557	1550	quinoline ip
1506	1504	quinoline ip	1541	1548	quinoline ip	1504	1503	quinoline ip	1505	1503	quinoline ip
1468	1482	ν(C=N(gua))	1506	1501	quinoline ip	1469	1474	ν(C=N(gua))	1468	1486	ν(C=N(gua))
1408	1409	guanidine ip A	1468	1474	ν(C=N(gua))		1415	guanidine ip A	1440	1430	quinoline ip
1381	1373	quinoline ip	1410	1415	guanidine ip A	1383	1348	δ(C–H(gua))	1415	1409	guanidine ip A
1331	1347	δ(C–H(gua))	1388	1345	δ(C–H(gua))	1304	1278	δ(C–H(Me))	1385	1374	quinoline ip
1302	1334	quinoline ip	1319	1335	δ(C–H(gua))		1266	δ(guanidine)	1329	1329	DBCat ip
1238	1260	δ(guanidine)	1300	1286	δ(C–H(Me)	1022	1044	guanidine ip B	1295	1305	ν(C–C(*t*Bu))
1026	1046	guanidine ip B	1236	1269	δ(guanidine)	974	992	δ(C–H(qu))	1278	1277	ν(C–C(*t*Bu))
858	873	δ(C–H(qu))	1024	1043	guanidine ip B	852	848	δ(C–H(Me))	1237	1237	ν(C–C(*t*Bu))
			825	849	δ(C–H(qu))				980	985	ν(C–O(DBCat))
									859	874	δ(C–H(qu))

[a] Abbreviations: ν, stretching; δ, deformation; ip, in-plane; qu, quinoline; gua, guanidine.

a significant enhancement of the accordance. Hence we report the frequencies without scaling.

Conclusion

The presented neutral Sn(IV) complexes are the first tin complexes with guanidine ligands. Thus we were able to show that guanidines are versatile ligands not only for transition metals but also for main group metals.

With the hybrid guanidine DMEGqu the complexes [Sn(DMEGqu)Cl_4] (**C1**), [Me_2Sn(DMEGqu)Cl_2] (**C2**) and [Me_2Sn(DMEGqu)Br_2] (**C3**) were crystallized. A reaction of 3,5-di-*tert*-butyl-*o*-benzoquinone with tin(II) chloride and the subsequent reaction with DMEGqu yielded crystals of the tin(IV) catecholate complex [Sn(DMEGqu)(3,5-DBCat)Cl_2] · 1.5THF (**C4**). In all complexes the Sn atom is six-coordinate with a slightly distorted octahedral configuration. The Sn–N bond lengths are in good accordance to reported complexes with quinoline and Schiff base ligands [9 – 12]. The Sn–N_{imine} bonds are shown to be considerably shorter than the Sn–N_{qu} bonds, thus proving the guanidine as the better *N*-donor for a central atom with a high positive formal charge like Sn(IV).

Additionally, a novel tin oxocluster [(Sn(DMEGqu)Br)$_4$(μ_2-O)$_4$(μ_2-OH)$_2$]Br_2 · 2MeCN (**C5**) was obtained with a structure where four Sn atoms are arranged in a distorted, adamantane-like cage, bridged by four oxido and two hydroxido ligands. Each tin(IV) center is additionally coordinated by the hybrid guanidine DMEGqu.

Selected complexes were modelled *via* density functional theory methods. In order to obtain a reasonable theoretical description, several functional/basis set combinations were evaluated. In spite of the simplicity of the ECP basis set combination LANL2DZ, it was found that the best description of the complexes **C1** and **C2** was achieved with B3LYP/LANL2DZ. A detailed computational analysis of the guanidine vibration modes within the complexes **C1**–**C4** has been provided.

Experimental Section

All reactions were carried out in a glove box or under Schlenk conditions in an inert gas atmosphere. All solvents were dried and degassed before utilization according to standard procedures [38]. The utilized chemicals were purchased

from the companies Fluka, Sigma-Aldrich, Acros and abcr, and were used without further purification.

Physical methods

Elemental analyses: Leco Instrument CHNS-932. Mass spectrometry (ESI): The electrospray mass spectra were collected on a TSQ Thermoquest Finnigan Instrument, with acetonitrile as mobile phase. Infrared spectroscopy: Spectra were collected on a Bruker IFS 28 Fourier spectrometer. – NMR spectroscopy of the presented complexes could not be carried out due to low solubility of the complexes.

General synthesis of Sn(IV) guanidine complexes

A solution of a tin(IV) halide SnX_2Y_2 (X = Cl or Me; Y = Cl or Br) (0.5 mmol) in dry MeCN was added to a solution of the DMEGqu ligand (0.5 mmol) in MeCN. Single crystals of the complexes [Sn(DMEGqu)Cl_4] (**C1**), [Me_2Sn(DMEGqu)Cl_2] (**C2**) and [Me_2Sn(DMEGqu)Br_2] (**C3**) were obtained by diffusion of diethyl ether.

*[Sn(DMEGqu)Cl_4] (**C1**)*

Yellow crystals, yield: 0.20 g (80 %), 500.83 g mol^{-1}. – IR (KBr, cm^{-1}): ν = 3059 w (ν(C–H)), 2962 w (ν(C–H)), 2931 w (ν(C–H)), 2891 w (ν(C–H)), 2802 vw (ν(C–H)), 1599 vs (ν(C–N_{imine})), 1554 vs, 1506 vs, 1468 s (ν(C=N_{imine})), 1429 w, 1408 m, 1398 s, 1381 vs, 1331 vs, 1302 s, 1238 s, 1213 m, 1174 m, 1140 w, 1107 m, 1084 m, 1053 m, 1026 m, 978 m, 949 m, 918 m, 858 s, 825 vs, 808 m, 777 s, 760 vs, 694 m, 656 w, 629 m, 606 w, 595 w, 580 m, 536 m, 519 w, 478 w, 453 w, 440 w. – $C_{14}H_{16}N_4Cl_4Sn$: calcd. C 33.6, H 3.2, N 11.2; found C 33.3, H 3.5, N 10.9. – MS ((+)-ESI): m/z (%) = 471.0 (< 5) [M–Cl = $C_{14}H_{16}N_4{}^{37}Cl_3{}^{120}Sn]^+$, 469.0 (5) [M–Cl = $C_{14}H_{16}N_4{}^{37}Cl_2{}^{35}Cl^{120}Sn$ = $C_{14}H_{16}N_4{}^{37}Cl_3{}^{118}Sn]^+$, 467.0 (10) [M–Cl = $C_{14}H_{16}N_4{}^{37}Cl^{35}Cl_2{}^{120}Sn$ = $C_{14}H_{16}N_4{}^{37}Cl_2{}^{35}Cl^{118}Sn$ = $C_{14}H_{16}N_4{}^{37}Cl_3{}^{116}Sn]^+$, 465.0 (16) [M–Cl = $C_{14}H_{16}N_4{}^{35}Cl_3{}^{120}Sn$ = $C_{14}H_{16}N_4{}^{37}Cl^{35}Cl_2{}^{118}Sn$ = $C_{14}H_{16}N_4{}^{37}Cl_2{}^{35}Cl^{116}Sn]^+$, 463.0 (10) [M–Cl = $C_{14}H_{16}N_4{}^{35}Cl_3{}^{118}Sn$ = $C_{14}H_{16}N_4{}^{37}Cl^{35}Cl_2{}^{116}Sn]^+$, 461.0 (5) [M–Cl = $C_{14}H_{16}N_4{}^{35}Cl_3{}^{116}Sn]^+$, 241.2 (100) [M–$SnCl_4$ + H = $C_{14}H_{17}N_4]^+$.

*[Me_2Sn(DMEGqu)Cl_2] (**C2**)*

Yellow crystals, yield: 0.12 g (53 %), 459.99 g mol^{-1}. – IR (KBr, cm^{-1}): ν = 3062 w (ν(C–H)), 3045 w (ν(C–H)), 3004 w (ν(C–H)), 2922 w (ν(C–H)), 2908 w (ν(C–H)), 2885 w (ν(C–H)), 2794 vw (ν(C–H)), 1595 s (ν(C–N_{imine})), 1574 vs, 1541 vs, 1506 vs, 1468 s (ν(C=N_{imine})), 1410 m, 1388 vs, 1319 s, 1300 m, 1236 m, 1211 w, 1174 w, 1167 w, 1134 w, 1103 m, 1049 w, 1024 m, 976 m, 908 w, 825 m, 804 m, 777 s, 766 m, 687 m, 660 w, 636 m, 606 w, 596 w, 579 m, 559 m, 534 w, 521 w, 471 w, 463 w, 447 w, 432 w. – $C_{16}H_{22}N_4Cl_2Sn$: calcd. C 41.8, H 4.8, N 12.2; found C 42.0, H 4.9, N 12.2. – MS ((+)-ESI): m/z (%) = 427.1 (<2) [M–Cl = $C_{16}H_{22}N_4{}^{37}Cl^{120}Sn]^+$, 425.1 (2) [M–Cl = $C_{16}H_{22}N_4{}^{35}Cl^{120}Sn$ = $C_{16}H_{22}N_4{}^{37}Cl^{118}Sn]^+$, 423.1 (< 2) [M–Cl = $C_{16}H_{22}N_4{}^{35}Cl^{118}Sn$ = $C_{16}H_{22}N_4{}^{37}Cl^{116}Sn]^+$, 421.1 (< 2) [M–Cl = $C_{16}H_{22}N_4{}^{35}Cl^{116}Sn]^+$, 241.2 (100) [M–$(CH_3)_2SnCl_2$ + H = $C_{14}H_{17}N_4]^+$.

*[Me_2Sn(DMEGqu)Br_2] (**C3**)*

Yellow crystals, yield: 0.15 g (55 %), 548.89 g mol^{-1}. – IR (KBr, cm^{-1}): ν = 3055 vw (ν(C–H)), 3033 vw (ν(C–H)), 3012 w (ν(C–H)), 2949 w (ν(C–H)), 2914 w (ν(C–H)), 2871 w (ν(C–H)), 2794 vw (ν(C–H)), 2781 vw (ν(C–H)), 1595 vs (ν(C–N_{imine})), 1552 s, 1504 m, 1469 m (ν(C=N_{imine})), 1425 w, 1410 m, 1383 s, 1327 s, 1304 s, 1238 m, 1215 m, 1176 m, 1140 w, 1103 m, 1082 w, 1043 w, 1022 m, 974 m, 910 vw, 879 vw, 852 m, 823 s, 806 s, 785 vs, 768 s, 758 s, 685 m, 654 w, 634 m, 596 m, 584 w, 561 m, 534 m, 509 w, 484 w, 447 w, 434 w. – $C_{16}H_{22}N_4Br_2Sn$: calcd. C 35.0, H 4.0, N 10.2; found C 35.0, H 4.1, N 10.2. – MS ((+)-ESI): m/z (%) = 471.1 (< 5) [M–Br = $C_{16}H_{22}N_4{}^{81}Br^{120}Sn]^+$, 469.1 (5) [M–Br = $C_{16}H_{22}N_4{}^{79}Br^{120}Sn$ = $C_{16}H_{22}N_4{}^{81}Br^{118}Sn]^+$, 467.1 (<5) [M–Br = $C_{16}H_{22}N_4{}^{79}Br^{118}Sn$ = $C_{16}H_{22}N_4{}^{81}Br^{116}Sn]^+$, 465.1 (<5) [M–Br = $C_{16}H_{22}N_4{}^{79}Br^{116}Sn]^+$, 241.2 (100) [M–$(CH_3)_2SnBr_2$ + H = $C_{14}H_{17}N_4]^+$.

Synthesis of the Sn(IV) catecholate-guanidine complex

In analogy to the synthesis described by Piskunov *et al.* [22], $SnCl_2$ (0.5 mmol) was added to a solution of 3,5-di-*tert*-butyl-*o*-benzoquinone (3,5-DBQ) (0.5 mmol) in tetrahydrofuran (THF), leading to the oxidation of Sn(II) to Sn(IV) and *in situ* generation of the [Sn(thf)$_2$(3,5-DBCat)Cl_2] complex with the dianion 3,5-di-*tert*-butylcatecholate (3,5-DBCat). The solution changed its color from dark purple to light yellow.

After adding the ligand DMEGqu (0.5 mmol) to the mixture, an orange solution was obtained, from which single crystals of the neutral complex [Sn(DMEGqu)(3,5-DBCat)Cl_2] · 1.5THF (**C4**) were isolated.

*[Sn(DMEGqu)(DBCat)Cl_2] · 1.5THF (**C4**)*

Yellow crystals, yield: 0.27 g (92 %), 650.23 g mol^{-1}. – IR (KBr, cm^{-1}): ν = 2951 m (ν(C–H)), 2900 m (ν(C–H)), 2863 m (ν(C–H)), 1597 s (ν(C–N_{imine})), 1557 s, 1505 m, 1468 m (ν(C=N_{imine})), 1440 m, 1415 s, 1385 vs, 1329 m, 1295 m, 1278 m, 1237 m, 1207 w, 1171 w, 1106 w, 1063 m, 1022 m, 980 m, 905 w, 859 m, 826 m, 808 m, 778 w, 760 m, 750 m, 694 w, 660 vw, 633 w, 621 w, 613 w, 597 w, 585 w, 536 w, 518 vw, 486 w, 444 w. –

Table 7. Crystal structure data for **C1–C5**.

	[Sn(DMEGqu)Cl_4] (**C1**)	[Me_2Sn(DMEGqu)Cl_2] (**C2**)	[Me_2Sn(DMEGqu)Br_2] (**C3**)	[Sn(DMEGqu)(DBCat)Cl_2] · 1.5THF (**C4**)	[(Sn(DMEGqu)Br)$_4$(μ-O)$_4$(μ-OH)$_2$]Br_2 · 2MeCN (**C5**)
Empirical formula	$C_{14}H_{16}N_4Cl_4Sn$	$C_{16}H_{22}N_4Cl_2Sn$	$C_{16}H_{22}N_4Br_2Sn$	$C_{28}H_{36}N_4Cl_2O_2Sn$	$C_{56}H_{66}N_{16}Br_6O_6Sn_4$
M_r	500.83	459.99	548.89	650.23	2013.49
Crystal size, mm^3	$0.24 \times 0.19 \times 0.13$	$0.26 \times 0.11 \times 0.04$	$0.16 \times 0.15 \times 0.13$	$0.21 \times 0.14 \times 0.09$	$0.31 \times 0.28 \times 0.05$
Crystal system	monoclinic	orthorhombic	orthorhombic	monoclinic	monoclinic
Space group	$P2_1/c$	$P2_12_12_1$	$P2_12_12_1$	$P2_1/c$	$C2/c$
a, Å	14.146(1)	7.850(1)	6.819(1)	9.158(1)	22.646(1)
b, Å	8.182(1)	14.688(1)	16.793(1)	14.827(1)	13.438(1)
c, Å	15.592(1)	16.234(1)	16.836(1)	26.712(2)	25.988(1)
β, deg	97.15(1)	90	90	103.25(1)	111.61(1)
Z	4	4	4	4	4
$D_{calcd.}$, g cm^{-3}	1.86	1.63	1.89	1.36	1.89
μ(MoK_α), mm^{-1}	2.0	1.7	5.5	0.9	4.7
F(000), e	984	920	1064	1488	4064
hkl range	$\pm17, \pm9, \pm18$	$-8/9, \pm17, -19/18$	$\pm8, -18/20, -19/20$	$\pm11, -17/16, \pm32$	$\pm27, \pm16, -31/29$
Refl. collected / unique / R_{int}	12500 / 3330 / 0.0320	8403 / 3476 / 0.0391	9632 / 3374 / 0.0358	22092 / 6565 / 0.0652	28136 / 6820 / 0.0459
Refined parameters	210	212	212	387	432
$R(F)$ / $wR(F^2)$ [$I > 2\,\sigma(I)$]	0.0200 / 0.0424	0.0281 / 0.0419	0.0234 / 0.0379	0.0372 / 0.0615	0.0316 / 0.0615
$R(F)$ / $wR(F^2)$ (all data)	0.0258 / 0.0431	0.0362 / 0.0427	0.0283 / 0.0382	0.0782 / 0.0648	0.0558 / 0.0636
x (Flack)	–	−0.03(2)	0.020(8)	–	–
GoF (F^2)	0.954	0.857	0.919	0.822	0.870
$\Delta\rho_{fin}$ (max / min), e $Å^{-3}$	0.337 / −0.360	0.621 / −0.375	0.598 / −0.353	0.726 / −0.517	1.316 / −0.716

$C_{34}H_{48}N_4Cl_2O_{3.5}Sn$: calcd. C 53.9, H 6.4, N 7.4; found C 53.6, H 6.5, N 7.1. – MS ((+)-ESI): m/z (%) = 650.2 (< 1) [M = $C_{28}H_{36}N_4^{35}Cl_2O_2{}^{120}Sn]^+$, 241.1 (100) [M–$C_{14}H_{20}O_2$–$SnCl_2$ + H = $C_{14}H_{17}N_4]^+$.

Using $SnBr_4$, orange crystals of [Sn(DMEGqu)Br_4] were obtained which were too small for X-ray analysis. Instead red crystals which precipitated from the solution on air were isolated in small yield. The complex was identified as the Sn(IV) oxocluster [(Sn(DMEGqu)Br)$_4$(μ_2-O)$_4$(μ_2-OH)$_2$]Br_2 · 2MeCN (**C5**).

Details of density functional theory calculations

All studies were carried out at the density functional level with the program GAUSSIAN 09 [39]. Employed functionals, basis sets and electronic core potentials are listed in the DFT section [28 – 34, 36]. For viewing and preparation purposes the program GAUSSVIEW 5.0 was used.

X-Ray structure determinations

Crystal data and numbers pertinent to data collection and structure refinement of the crystal structure determinations of the complexes [Sn(DMEGqu)Cl_4] (**C1**), [Me_2Sn(DMEGqu)Cl_2] (**C2**), [Me_2Sn(DMEGqu)Br_2] (**C3**), [Sn(DMEGqu)(DBCat)Cl_2] (**C4**) and [(Sn(DMEGqu)Br)$_4$(μ_2-O)$_4$(μ_2-OH)$_2$]Br_2 (**C5**) are summarized in Table 7. Data were collected on an Oxford Diffraction XcaliburS diffractometer using the Programs CRYSALIS and CRYSALIS RED [40]. The structures were solved using Direct Methods (SHELX-90) [41], structural refinement was done with SHELXL-97 [42]. In **C4** one half THF molecule was found to be disordered. As it was not possible to model the disordered solvent molecule in an adequate manner, the data set was treated with the routine SQUEEZE of PLATON [43, 44].

CCDC 926299 (**C1**), 926300 (**C2**), 926301 (**C3**), 926302 (**C4**) and 926303 (**C5**) contain the supplementary crystallographic data for this paper. These data can be obtained free of charge from The Cambridge Crystallographic Data Centre *via* www.ccdc.cam.ac.uk/data_request/cif.

Acknowledgement

Financial support by the Fonds der Chemischen Industrie (fellowship for S. H.-P.), the Bundesministerium für Bildung und Forschung (MoSGrid, 01IG09006) and the Deutsche Forschungsgemeinschaft is gratefully acknowledged. Calculation time is gratefully acknowledged from the ARMINIUS Cluster at the PC^2 Paderborn. The authors thank Prof. K. Jurkschat for his valuable support.

[1] I. R. Beattie, M. Milne, M. Webster, H. E. Blayden, P. J. Jones, R. Killean, J. L. Laurence, *J. Chem. Soc. A* **1969**, 482.
[2] V. J. Hall, E. Tiekink, *Z. Kristallogr.* **1996**, *211*, 247.
[3] T. A. Kabanos, A. D. Keramidas, D. Mentzafos, U. Russo, A. Terzis, J. M. Tsangaris, *J. Chem. Soc., Dalton Trans.* **1992**, 2729.
[4] C. Pettinari, M. Pellei, A. Cingolani, D. Martini, A. Drozdov, S. Troyanov, W. Panzeri, A. Mele, *Inorg. Chem.* **1999**, *38*, 5777.
[5] B. Yearwood, S. Parkin, D. A. Atwood, *Inorg. Chim. Acta* **2002**, *333*, 124.
[6] N. J. Hill, G. Reeske, J. A. Moore, A. H. Cowley, *Dalton Trans.* **2006**, 4838.
[7] D. P. Arnold, J. Blok, *Coord. Chem. Rev.* **2004**, *248*, 299.
[8] T. Kojima, K. Hanabusa, K. Ohkubo, M. Shiro, S. Fukuzumi, *Chem. Eur. J.* **2010**, *16*, 3646.
[9] K. Takano, M. Takahashi, T. Fukushima, M. Takezaki, T. Tominaga, H. Akashi, H. Takagi, T. Shibahara, *Bull. Chem. Soc. Jpn.* **2012**, *85*, 1210.
[10] A. Chaudhary, R. V. Singh, *Main Group Met. Chem.* **2008**, *31*, 107.
[11] D. K. Manju, K. Dinesh, *J. Coord. Chem.* **2011**, *64*, 2130.
[12] A. K. Singh, S. Bhandari, *Main Group Met. Chem.* **2003**, *26*, 155.
[13] D. Stalke, M. A. Paver, D. S. Wright, *Angew. Chem., Int. Ed. Engl.* **1993**, *32*, 428.
[14] S. R. Foley, G. P. A. Yap, D. S. Richeson, *Polyhedron* **2002**, *21*, 619.
[15] W. Kantlehner, E. Haug, W. Mergen, P. Speh, T. Maier, J. Kapassakalidis, H. Bräuner, H. Hagen, *Liebigs Ann. Chem.* **1984**, 108.
[16] S. Herres-Pawlis, U. Flörke, G. Henkel, *Eur. J. Inorg. Chem.* **2005**, 3815.
[17] S. Herres-Pawlis, A. Neuba, O. Seewald, T. Seshadri, H. Egold, U. Flörke, G. Henkel, *Eur. J. Org. Chem.* **2005**, 4879.
[18] A. Neuba, R. Haase, M. Bernard, U. Flörke, S. Herres-Pawlis, *Z. Anorg. Allg. Chem.* **2008**, *634*, 2511.
[19] O. Bienemann, A. Hoffmann, S. Herres-Pawlis, *Rev. Inorg. Chem.* **2011**, *31*, 83.
[20] J. Börner, U. Flörke, K. Huber, A. Döring, D. Kuckling, S. Herres-Pawlis, *Chem. Eur. J.* **2009**, *15*, 2362.
[21] A. Hoffmann, J. Börner, U. Flörke, S. Herres-Pawlis, *Inorg. Chim. Acta* **2009**, *362*, 1185.
[22] A. V. Lado, A. I. Poddel'sky, A. V. Piskunov, G. K. Fukin, E. V. Baranov, V. N. Ikorskii, V. K. Cherkasov, G. A. Abakumov, *Inorg. Chim. Acta* **2005**, *358*, 4443.

[23] V. Raab, K. Harms, J. Sundermeyer, B. Kovacevic, Z. Maksic, *J. Org. Chem.* **2003**, *68*, 8790.
[24] K. Ray, T. Petrenko, K. Wieghardt, F. Neese, *Dalton Trans.* **2007**, 1552.
[25] H. Berwe, A. Haas, *Chem. Ber.* **1987**, *120*, 1175.
[26] R. M. Harker, M. F. Mahon, K. C. Molloy, *Main Group Met. Chem.* **1996**, *19*, 29.
[27] K. Wraage, T. Pape, R. Herbst-Irmer, M. Noltemeyer, H.-G. Schmidt, H. W. Roesky, *Eur. J. Inorg. Chem.* **1999**, 869.
[28] A. D. Becke, *Phys. Rev A* **1988**, *38*, 3098.
[29] C. Lee, W. Yang, R. G. Parr, *Phys. Rev. B* **1988**, *32*, 785.
[30] J. P. Perdew, *Phys. Rev. B* **1986**, *33*, 8822.
[31] A. D. Becke, *J. Chem. Phys.* **1993**, *98*, 5648.
[32] R. Ahlrichs, M. Bär, M. Häser, H. Horn, C. Kölmel, *Chem. Phys. Lett.* **1989**, *162*, 165.
[33] F. Weigend, R. Ahlrichs, *Phys. Chem. Chem. Phys.* **2005**, *7*, 3297.
[34] P. J. Hay, W. R. Wadt, *J. Chem. Phys.* **1985**, *82*, 284.
[35] J. Martin, A. Sundermann, *J. Chem. Phys.* **2001**, *114*, 3408.
[36] M. J. Frisch, J. A. Pople, J. S. Binkley, *J. Chem. Phys.* **1984**, *80*, 3265.
[37] C. J. Cramer, *Essentials of Computational Chemistry*, Wiley, Chichester, **2004**, p. 340.
[38] J. Leonard, B. Lygo, G. Procter, *Praxis der Organischen Chemie*, VCH, Weinheim, **1996**.
[39] M. J. Frisch, G. W. Trucks, H. B. Schlegel, G. E. Scuseria, M. A. Robb, J. R. Cheeseman, G. Scalmani, V. Barone, B. Mennucci, G. A. Petersson, H. Nakatsuji, M. Caricato, X. Li, H. P. Hratchian, A. F. Izmaylov, J. Bloino, G. Zheng, J. L. Sonnenberg, M. Hada, M. Ehara, K. Toyota, R. Fukuda, J. Hasegawa, M. Ishida, T. Nakajima, Y. Honda, O. Kitao, H. Nakai, T. Vreven, J. A. Montgomery, Jr., J. E. Peralta, F. Ogliaro, M. Bearpark, J. J. Heyd, E. Brothers, K. N. Kudin, V. N. Staroverov, T. Keith, R. Kobayashi, J. Normand, K. Raghavachari, A. Rendell, J. C. Burant, S. S. Iyengar, J. Tomasi, M. Cossi, N. Rega, J. M. Millam, M. Klene, J. E. Knox, J. B. Cross, V. Bakken, C. Adamo, J. Jaramillo, R. Gomperts, R. E. Stratmann, O. Yazyev, A. J. Austin, R. Cammi, C. Pomelli, J. W. Ochterski, R. L. Martin, K. Morokuma, V. G. Zakrzewski, G. A. Voth, P. Salvador, J. J. Dannenberg, S. Dapprich, A. D. Daniels, O. Farkas, J. B. Foresman, J. V. Ortiz, J. Cioslowski, D. J. Fox, GAUSSIAN 09 (revision B.01), Gaussian, Inc., Wallingford CT (USA) **2010**.
[40] CRYSALIS CCD and CRYSALIS RED, Oxford Diffraction Ltd., Abingdon, Oxford (U. K.) **2008**.
[41] G. M. Sheldrick, *Acta Crystallogr.* **1990**, *A46*, 467.
[42] G. M. Sheldrick, *Acta Crystallogr.* **2008**, *A64*, 112.
[43] A. L. Spek, PLATON, A Multipurpose Crystallographic Tool, Utrecht University, Utrecht (The Netherlands) **2008**.
[44] A. L. Spek, *J. Appl. Crystallogr.* **2009**, *D65*, 148.